Controlling Transient Thermal Effects in High-Power Gravitational-Wave Detectors

Arnaldo Rodríguez González

Mentor: Dr. Aidan Brooks

LIGO Laboratory,

California Institute of Technology

Abstract

Detecting gravitational waves from high-frequency emitters (such as black hole collisions) requires gravitational-wave detectors with high operating laser powers; these cause thermal effects in the test-masses that deteriorate control signals and decrease interferometer sensitivity. To correct these, a prototype control system model was developed for Advanced LIGO's thermal compensation system to reduce optical wavefront distortion from thermal lensing and surface deformation. A finite element model of the heating in the test-mass was developed in COMSOL to interact dynamically with the control system developed in MATLAB, as well as a linearized time-efficient heating model using only MATLAB. We analyzed data from both models and from experiment to verify the system's behavior and validate the control system model's integrity.

I. BACKGROUND

The LIGO detectors, located in Washington and Louisiana, are power-recycled Michelson interferometers with Fabry–Pérot cavities located at the detector's "arms". Advanced LIGO has been designed to be ten times more sensitive in the high-frequency range of gravitational waves compared to the initial LIGO detectors. To accomplish this, the laser power in the interferometers has been increased significantly from the initial power configuration. The thermal effects generated in the test-masses[1]as a result of this are addressed and corrected through a thermal compensation system, or TCS. This system needs to be as efficient as possible and to interfere as little as possible with the rest of the interferometer's systems.

These effects can be categorized as thermorefractive and thermoelastic; the former due to temperature-dependent refractive indices in the test mass substrate, and the latter due to surface deformation as a result of uneven thermal expansion. Both of these effects generate wavefront distortion on the interferometer beams, which lead to signal degradation and higher-order mode loss in the Fabry-Pérot cavity.

The magnitude of these lenses can be quantified by assuming they are nearly quadratic and then calculating the wavefront's quadratic coefficient, or defocus. The equations for calculating the thermorefractive and thermoelastic defocus (a_r and a_e respectively) are shown in Eq. I.1 and I.2, where $T(r,z,t)$ is the temperature field, t is time, r is radial distance, z is height, ω_0 is the beam width (54 mm), $\frac{dn}{dT}$ is the thermo-optic coefficient, and $d(r,t)$ is the surface deformation field.

$$a_r(t) = \frac{-2[\frac{dn}{dT}\int_0^{z_0} T(\omega_0,z,t)dz - \frac{dn}{dT}\int_0^{z_0} T(0,z,t)dz]}{\omega_0^2} \tag{I.1}$$

$$a_e(t) = \frac{2[d(\omega_0,t) - d(0,t)]}{\omega_0^2} \tag{I.2}$$

The TCS is designed to correct these thermal lenses by inducing compensating thermal lenses in the test mass that eventually cancel out any optical aberrations present.

The TCS consists of two actuators and a sensor, working in tandem to allow controlled high-power operation by reducing the optical distortion in the system. These actuators perform different roles in the system: The ring heater, attached directly to the test mass, corrects thermoelastic effects in the test-masses, while the CO_2 laser, which is fired at a compensation plate located close to the test mass, is meant to correct thermorefractive effects. These effects are then measured by a Hartmann wavefront sensor.

II. FINITE ELEMENT MODEL

An axisymmetric finite element model of the input test mass (ITM) with the ring heater was developed in COMSOL, shown in Fig. II.1. The main laser beam and the ring heater were modeled as heat fluxes to study the transient thermal properties of the system. All material thermal properties are assumed to be the properties of Corning 7940 fused silica glass as preset by COMSOL, with the exception of the coefficient of thermal expansion (which was taken to be $5.7*10^{-7}$ K^{-1} due to an invalid COMSOL preset value)[2].

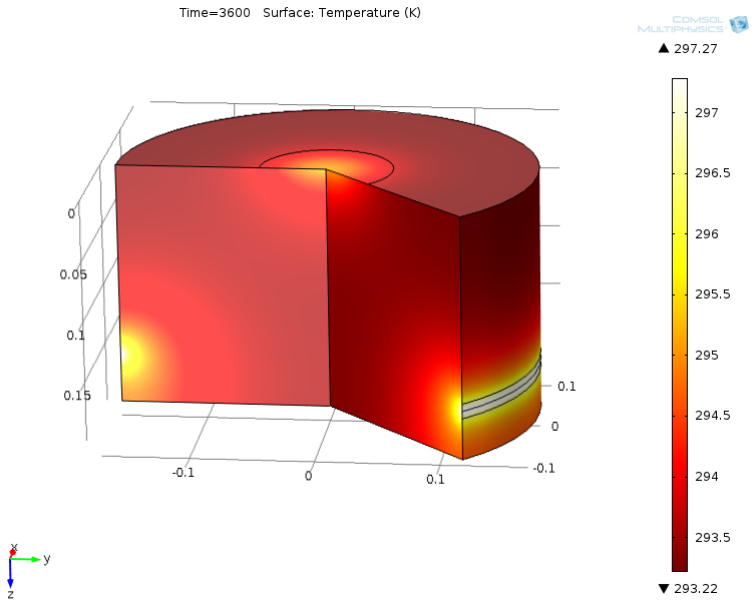

Figure II.1: An exemplary simulation result in which the main laser emits a total power of 0.5 W into the test mass and the ring heater emits a total of 5 W.

The model was tested for numerical stability and proper convergence in order to validate subsequent results. Mesh discretizations of different degrees of refinement were utilized in order to test the spatial frequency of the problem (not large in theory); the relative error calculated between results from standard and refined mesh settings was less than 0.005%, and it was subsequently determined that the model gave satisfactory results with a COMSOL standard mesh. Afterwards, the COMSOL model was exported as COMSOL+MATLAB code to enable manual alterations and the insertion of a PID control system; identical tests were run on the COMSOL+MATLAB equivalent and the original COMSOL model to conclude that the code produced valid results. Results from these identical tests agreed to a relative error of 0.01%, which was deemed acceptable.

The control system itself is a PID-type controller, which corrects error by utilizing three different parameters; proportional, integral, and derivative. (A block diagram of this controller is shown in Fig. II.2). The error function $e(t)$ in this case is simply the expected value of defocus, or setpoint, minus the actual value of the defocus a_e or a_r in the test mass (in diopters). The actuator function $u(t)$ gives the total power in watts that the ring heater applies as a function of time. This actuator function is the sum of the three components, where K_p is the proportional gain (in units of watt-meters), K_i is the integral gain (in units of watt-meters per second), and K_d is the derivative gain (in units of joule-meters.) The proportional signal corrects present error, the integral corrects the accumulation of past errors, and the derivative attempts to prevent future error.

A series of parameter studies were conducted on the controller model to conclusively verify

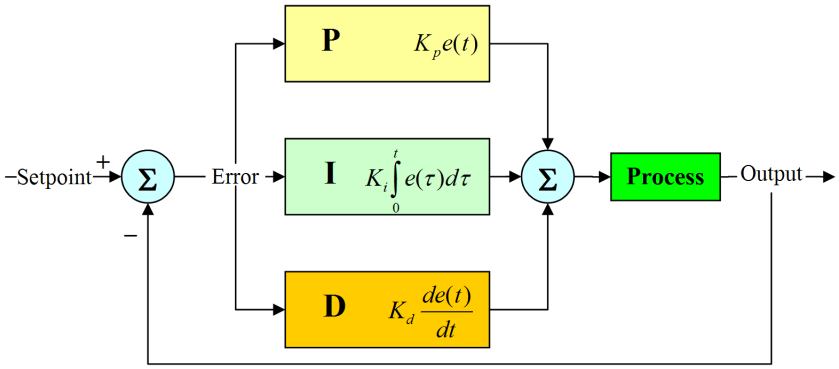

Figure II.2: A block diagram of an exemplary PID loop equivalent to the one utilized in our simulation.

if it was functioning correctly; individual sections of the PID controller were turned on and tested at a range of gains with the COMSOL+MATLAB code to ensure that the output behavior matched theory qualitatively, which it did. Subsequently, optimal gain parameters were calculated for the system as prescribed by both the Ziegler-Nichols and Tyreus-Luyben methods[3][4]. Both of these methods are heuristic in nature, and are rooted in the calculation of the minimum proportional gain that causes the output to oscillate regularly when only the proportional component of the controller is active. This value (and the output's oscillation period) are then used to calculate the system's gains.

To analyze the performance of these methods (and of the PID in general), self-heating from the main beam was applied to the ITM's finite element model (shown in Fig. II.1)

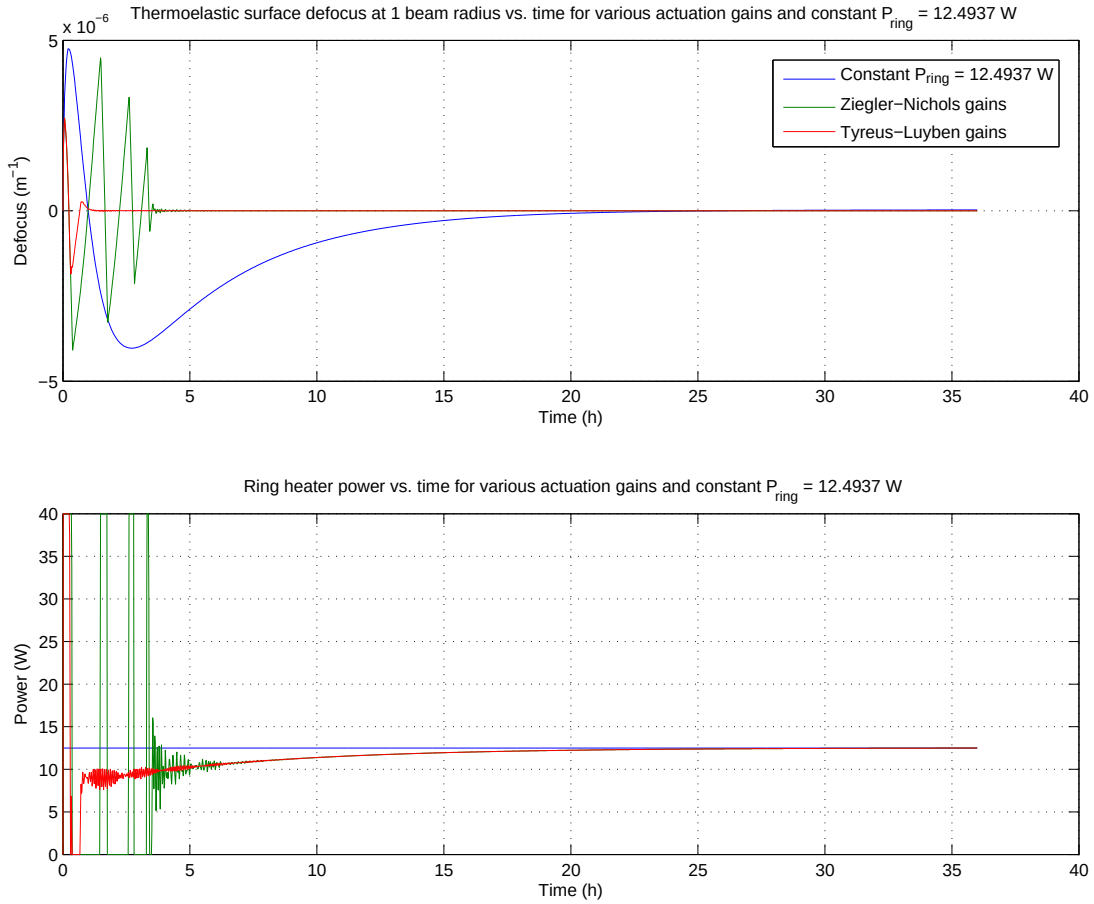

Figure II.3: A thermoelastic defocus & ring heater power comparison plot for active PID correction and passive constant-power correction. $K_{p_{ZN}} = -467856$ W·m, $K_{i_{ZN}} = -649.8$ W·m·s^{-1}, $K_{d_{ZN}} = -23.3928 * 10^7$ J·m, $K_{p_{TL}} = -243675$ W·m, $K_{i_{TL}} = -76.918$ W·m·s^{-1}, $K_{d_{TL}} = -10.6939 * 10^7$ J·m.

from $t = 0$. The thermoelastic defocus was used as the input for the PID loop (with gain parameters chosen according to the applied tuning method), and the output was used to drive the applied ring heater power as a function of time. A comparison plot of defocus with both Ziegler-Nichols and Tyreus-Luyben gains as well as constant-power correction is shown in Fig. II.3. As can be seen in Fig. II.3, the defocus reaches the setpoint nearly 5 times faster (or 16 hours earlier) than the passive constant-power case for Ziegler-Nichols gains, and reaches the setpoint 20 times faster (or 19 hours earlier) than the constant-power case for Tyreus-Luyben gains. This is expected, as Tyreus-Luyben gains are generally better suited than Ziegler-Nichols gains for systems where the input/output phase lag is small (due to a smaller proportional gain and higher integral/derivative gains).

III. THE WAVEFRONT PREDICTOR

Calculating solutions in COMSOL+MATLAB by using finite element analysis for both thermoelastic and thermorefractive effects increases the solving time : attempting to run parameter studies with the previous method is very inefficient, with solving times in the order of days for a single analysis. To skip the finite element analysis altogether, a wavefront predictor program in was developed in MATLAB.

The wavefront predictor operates by utilizing the principle of superposition; the sum of two individual solutions to the heat equation for given applied powers at applied times is the solution for the sum of both applied powers. Therefore, by utilizing the unit pulse wavefront response $W_\delta = W_H(r,t) - W_H(r,t+\Delta t)$ (where W_H is the unit step wavefront response) for both the laser and the ring heater, and adding appropriately time-shifted and scaled versions of it to itself, we can recreate the response to a series of applied powers without having to perform finite element analysis (except once, while calculating the response used to calculate the unit pulse response). The wavefront predictor serves to reduce the solving time from around the order of days to the order of minutes; a flowchart summarizing the predictor's method of operation is presented in Figure III.1.

The wavefront predictor's critical operating condition is that the heat equation can be approximated well as a linear inhomogeneous differential equation; the only nonlinear term present in the real model is the radiation boundary condition, which is described by the Stefan-Boltzmann law corrected for emissivity (Eq. III.1)

$$h = \varepsilon\sigma(T^4 - T_{ext}^4) \tag{III.1}$$

where h represents the outwards heat flux, ε represents the emissivity (0.9), σ is the Stefan-Boltzmann constant, T is the temperature, and T_{ext} is the external or ambient temperature. However, since $\frac{T-T_{ext}}{T} \ll 1$ for essentially every possible case to be analyzed, the linear term in the Taylor expansion of Eq. III.1 dominates and the boundary condition effectively becomes Equation III.2, which is linear. For cases where a large amount of power is being applied over large spans of time, however, this assumption is not necessarily valid and nonlinear radiation effects must be taken into account.

$$h = 4\varepsilon\sigma T_{ext}^3(T - T_{ext}) \tag{III.2}$$

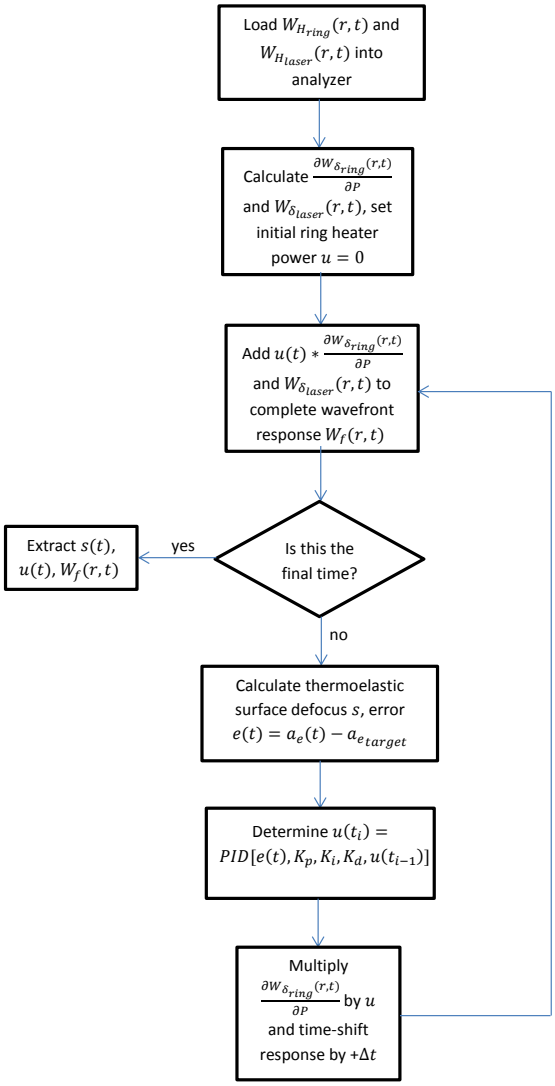

Figure III.1: A flowchart describing the wavefront predictor's method of operation.

The error produced by this linear approximation was quantified by calculating the relative error in steady-state defocus between the predictor and COMSOL using identical, constant powers. A plot of the relative error in both thermoelastic and thermorefractive defocus as a function of constant applied power from these tests is shown in Fig. III.2. The relative error passes 1% at a constant applied power of approximately 5 to 7 W for both types of defocus; this source of error needs to be recognized when using results from the predictor for tests that utilize an average of applied power larger than 5-7 W.

Using the wavefront predictor, a test similar to the one demonstrated in Fig. II.3 was conducted to compare active PID correction and passive constant-power correction by utilizing wavefront data from the finite element model described in Section II. The results from this test are illustrated in Fig. III.3; since both Ziegler-Nichols and Tyreus-Luyben gains created uncontrolled oscillations in the system, a heavily modified version of these was utilized

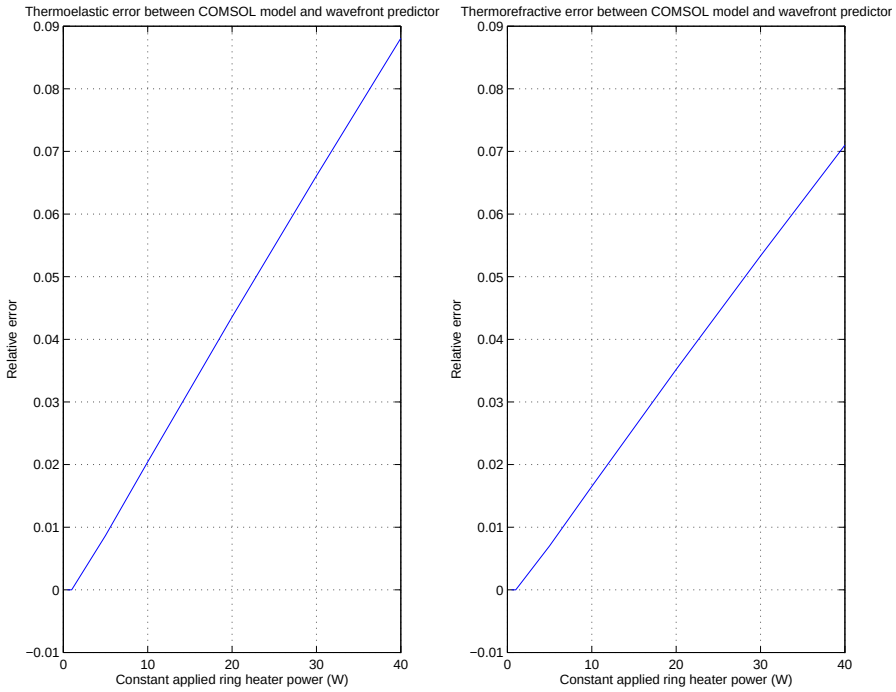

Figure III.2: Relative error between predictor and COMSOL+MATLAB models of steady-state thermoelastic & thermorefractive defocus as a function of constant applied powers.

based on trial-and-error methods. As can be seen, the PID controller eliminates defocus approximately 13.3 times faster (or 18.5 hours earlier) than the passive constant-power case for the applied gains.

IV. MODELS VS. EXPERIMENT

A. Thermally Altered Model & Steady-State Power Comparison

To verify the validity of the finite element model described in Section II, we compared defocus data[5] from a ring heater test at the LIGO Livingston Observatory (LLO) to data from the finite element model described previously, as seen in Fig. IV.1. A ring heater power of 6.3 W was applied at $t = 0$ for both cases and the defocus was measured as a function of time; as can be seen, there is a significant discrepancy between experimental data and the model as-is. The actual defocus value starts to rise approximately 15 minutes after the modeled value, and reaches its maximum 45 minutes from the modeled one. In an attempt to obtain a model that matched the transient behavior in the interferometer as closely as possible, an alternate finite element model was developed to best "fit" the modeled data to experiment. This was accomplished in two ways;

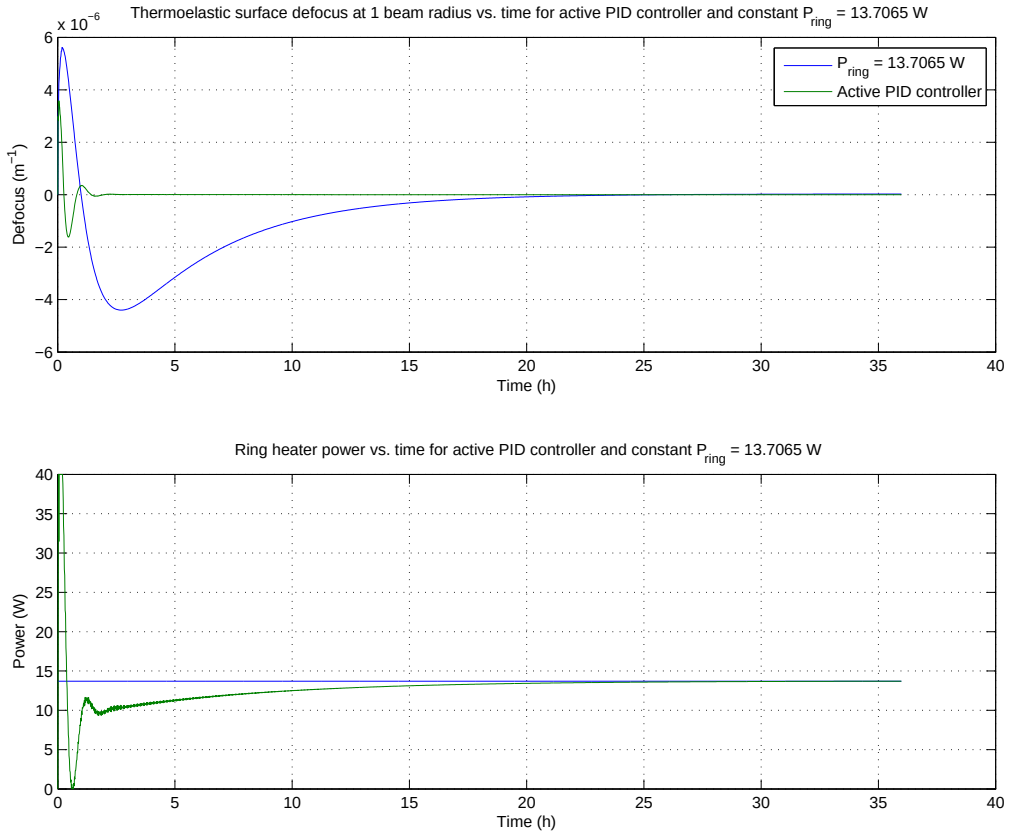

Figure III.3: Thermoelastic surface defocus and applied ring heater power as a function of time for active PID controller correction and passive constant-power correction cases. $K_p = -1 * 10^7$W·m, $K_i = -0.001714 * 10^7$ W·m·s^{-1}, $K_d = -125 * 10^7$ J·m.

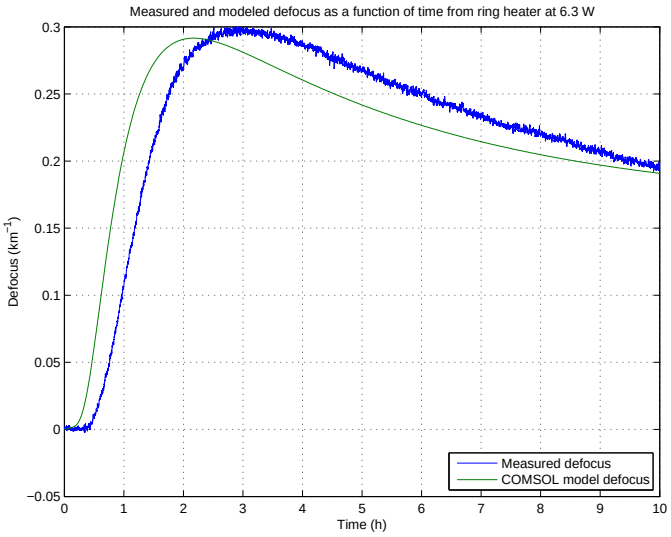

Figure IV.1: Comparison between model described in Section 3.1 and experimental data from RH test at LLO for identical input power of 6.3 W.

	Original Model	Thermally Fitted Model
τ	0 s	1200 s
C_p	Corning fused silica glass (7940)	770 J/(kg K)
k	Corning fused silica glass (7940)	1.31 W/(m K)
α	5.7×10^{-7} K^{-1}	5.7×10^{-7} K^{-1}

Table I: Comparison of thermal parameters between original and thermally altered model. Note: values for Corning fused silica glass are preset in COMSOL and are temperature-dependent functions.

- By adding a turn-on time constant to the ring heater. Realistically, due to the thermoelectric nature of the ring heater, it cannot emit at full power instantaneously; it requires a certain amount of time to "turn on". This was modeled by multiplying the ideal power that would be emitted by the ring heater with a $1 - e^{-t/\tau}$ term, where τ is the aforementioned time constant.

- By altering the material's thermal parameters to change the model's response. The parameters considered were the coefficient of thermal expansion α, the heat capacity at constant pressure C_p, and the thermal conductivity k.

Performing a parameter study by varying these four quantities allowed for the creation of a model whose behavior closely matches that of experiment. Precedent was given to models whose properties differed less to the original's since actual values are not expected to differ much from the material's standard properties. The altered model matches the experimental data very closely; a comparison graph of the altered model is shown in Fig. IV.2, while a table comparing thermal parameters for the original and altered model is shown in Table I. Note, however, the deviation from model & experiment behavior starting at approximately 7.5 hours; in spite of all efforts to find a set of thermal parameters that would not cause this discrepancy, this characteristic difference between model and experiment remained. This suggests the possibility of a discrepancy between model and experiment that is not associated with the test mass's material properties. The difference between the original thermal parameters and the fitted ones is not large; the value of Corning 7940 fused silica glass's thermal conductivity at room temperature is 1.38 W/(m K), which to the fitted model represents a reduction of approximately 5.07%. The specific heat capacity, although

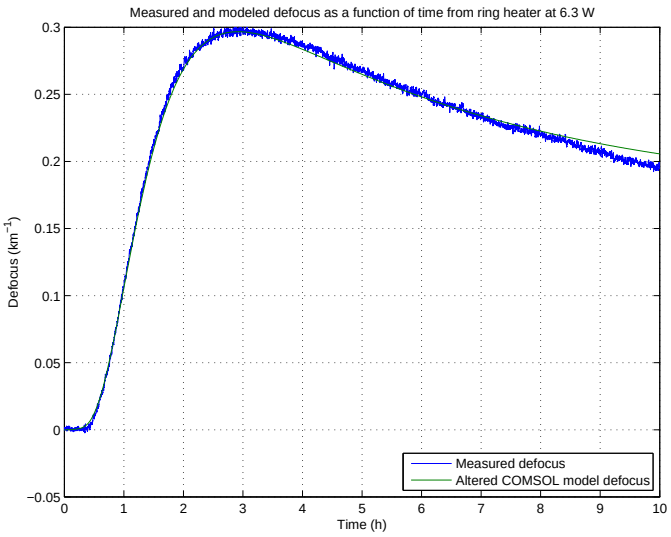

Figure IV.2: Comparison between the thermally altered model and experimental data from RH test at LLO for identical input power of 6.3 W.

set to the same value of Corning fused silica at room temperature, is now a fixed value and no longer temperature-dependent; the COMSOL fused silica default value varies less than a percent throughout the model's temperature ranges, but fixing the value still causes a discernible change in behavior.

B. Transient Controller-Active Comparison

After designing this thermally "fitted" model, we tested its validity by comparing its performance to experiment in a case where the input powers vary over time; i.e. when the controller is active. A set of input powers were calculated using the wavefront predictor described in Section III and finite element analysis data from the thermally fitted model; these were then given to the actual ring heater at the LLO, and the change in beam size was then measured over a period of time. A comparison graph of both of these is shown in Fig. IV.3; a significant section of this data is corrupted, as a magnitude 6.2 earthquake off the coast of Acapulco knocked the interferometer optics out of a stable configuration. In spite of this, there is a clear difference between the model and the experiment; the experiment seems to react quicker than the model, and appears to have a larger instantaneous oscillation amplitude than the model's. This causes a deviation that (as can be seen from Fig. IV.3) becomes more significant over time.

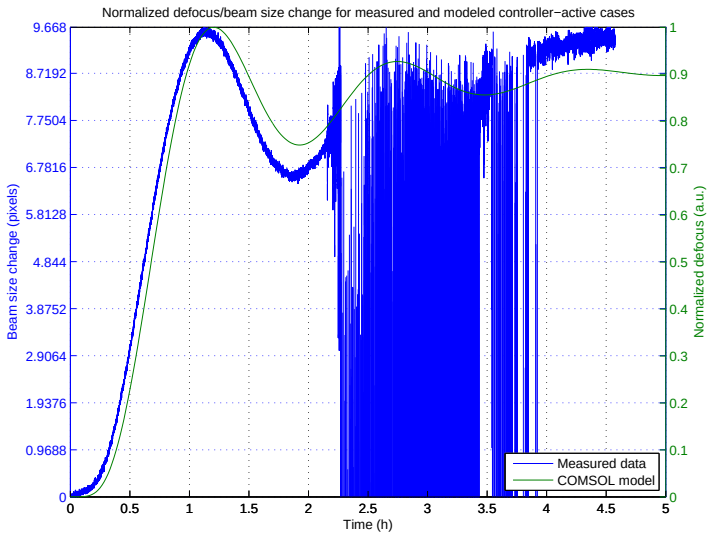

Figure IV.3: Normalized defocus and beam size change for thermally altered model and experimental data from controller-active RH test at LLO for identical varying input powers. Note the data corruption present due to the magnitude 6.2 earthquake off the coast of Acapulco.

V. FUTURE WORK

A. Quantifying Higher-Order Mode Losses

Equations I.1 & I.2 serve to define the defocus as an approximation based on data extracted from two points; however, by utilizing an alternate (albeit more computationally demanding) definition of the defocus, we can both optimize the aberration corrections and quantify higher-order mode losses in the Fabry-Pérot cavities. This method of defocus calculation is provided by Arain et al.[6] in one dimension, which involves calculating the maximum value of the overlap integral between the incident electric field on the test-mass's surface and an "optimal" incident electric field generated by a perfectly Gaussian beam. This overlap integral, which quantifies the amplitude coupling of these two fields, is defined in Equation V.1 for two-dimensional axisymmetric electric fields where $W(r)$ is the optical wavefront and λ is the beam wavelength (1064 nm).

$$I = 2\pi \left(\frac{2}{\pi\omega_0^2}\right) \int_0^\infty r e^{\frac{-2r^2}{\omega_0^2}} e^{\frac{4\pi i}{\lambda}(W(r)-ar^2)} dr \tag{V.1}$$

When the value of the integral I reaches its maximum, the entirely parabolic "optimal" aberration matches the actual aberration as closely as possible, indicating the best value

of defocus that characterizes the real aberration. In the current version of the program, this value is calculated through a section search algorithm that finds the maximum I value with the actual wavefront aberration data and extracts the corresponding defocus used to calculate it.

As well as providing a more comprehensive analysis of the defocus present in the test mass due to thermal effects, it can also help to quantify amplitude losses due higher-order transverse electromagnetic mode (TEM) matching in the cavity. Currently, an algorithm that uses Equation V.1 has been both developed and tested to work with the PID controller model and finite element model; however, quantifying amplitude losses directly has yet to be performed.

B. Complete TCS Finite Element Model

In order to fully simulate the TCS, a model has been developed that simulates both the ring heater and the CO_2 laser thermal effects on the test mass. The compensation plate has been added to the model's geometry, and the CO_2 laser is modeled as a heat flux incident on its surface. However, the addition of the compensation plate requires simulating surface-to-surface radiation effects between the plate and the test mass as well as coupled thermorefractive/thermoelastic effects, which severely slows down computational time. Due to this, the model has not yet been tested for validity. Testing the wavefront compiler's results using data from this model is a high priority; as radiation effects become more significant to the behavior of the test mass, error from the linear radiation approximation becomes larger, leading to larger deviations between model and experiment.

Acknowledgments

Dr. Aidan Brooks, for his patience and dedication to me & my project.

The LIGO SURF program, for giving me this opportunity to perform groundbreaking research at the forefront of science.

Caltech, for accommodating me so well during my research.

NSF, for funding programs and experiments like these.

---

[1] Chakraborty, R., Brooks, A., *Interferometer Response to TCS Perturbations*, LIGO-T1200100-v1, 2012.

[2] Valley Design Corporation, *Thermal/Mechanical Properties of Corning UV Grade Fused Silica*, United States of America, 2013.

[3] Ziegler, J.G., Nichols, N. B., *Optimum settings for automatic controllers*, Transactions of the ASME, United States of America, 1942.

[4] Shahroki, M., Zommorodi, A., *Comparison of PID controller tuning methods*, Sharif University of Technology, Iran, 2012.

[5] Brooks, A., *One Arm Test of Defocus Data*, e-mail correspondence to Arnaldo Rodríguez, August 13 2013.

[6] Arain, M., Quetschke, V., Gleason, J., Williams, L., Rakhmanov, M., Lee, J., Cruz, R., Mueller, G., Tanner, D., Reitze, D., *Adaptive beam shaping by controlled thermal lensing in optical elements*, Optical Society of America, United States of America, 2007.

[7] Ogata, K., *Modern Control Engineering*, Prentice-Hall, United States of America, 1982.

[8] Brooks, A., *Thermal Compensation for Advanced LIGO*, LIGO-G1300218-v1, 2013.

[9] Fricke, T., *Perl PID servo documentation*, LIGO log entry, 2009.

[10] Ballmer, S., *LIGO interferometer operating at design sensitivity with application to gravitational radiometry*, Massachusetts Institute of Technology, United States of America, 2006.

[11] Morrison, E., Meers, B., Robertson, D., Ward, H., *Automatic alignment of optical interferometers*, University of Glasgow, Scotland, 1993.

[12] Hello, P., Vinet, J., *Analytical models of thermal aberrations in massive mirrors heated by high power laser beams*, Université Paris-Sud, France, 1990

[13] Barsotti, L., Evans, M., Fritschel, P., *Alignment sensing and control in Advanced LIGO*, Massachusetts Institute of Technology, United States of America, 2009.

[14] Arain, M., Mueller, G., *Optical Layout and Parameters for the Advanced LIGO Cavities*, LIGO-T0900043-10, 2009.